CHEMISTRY OF MATERIALS

FEBRUARY 27, 2024 | VOLUME 36 | NUMBER 4 | pubs.acs.org/cm

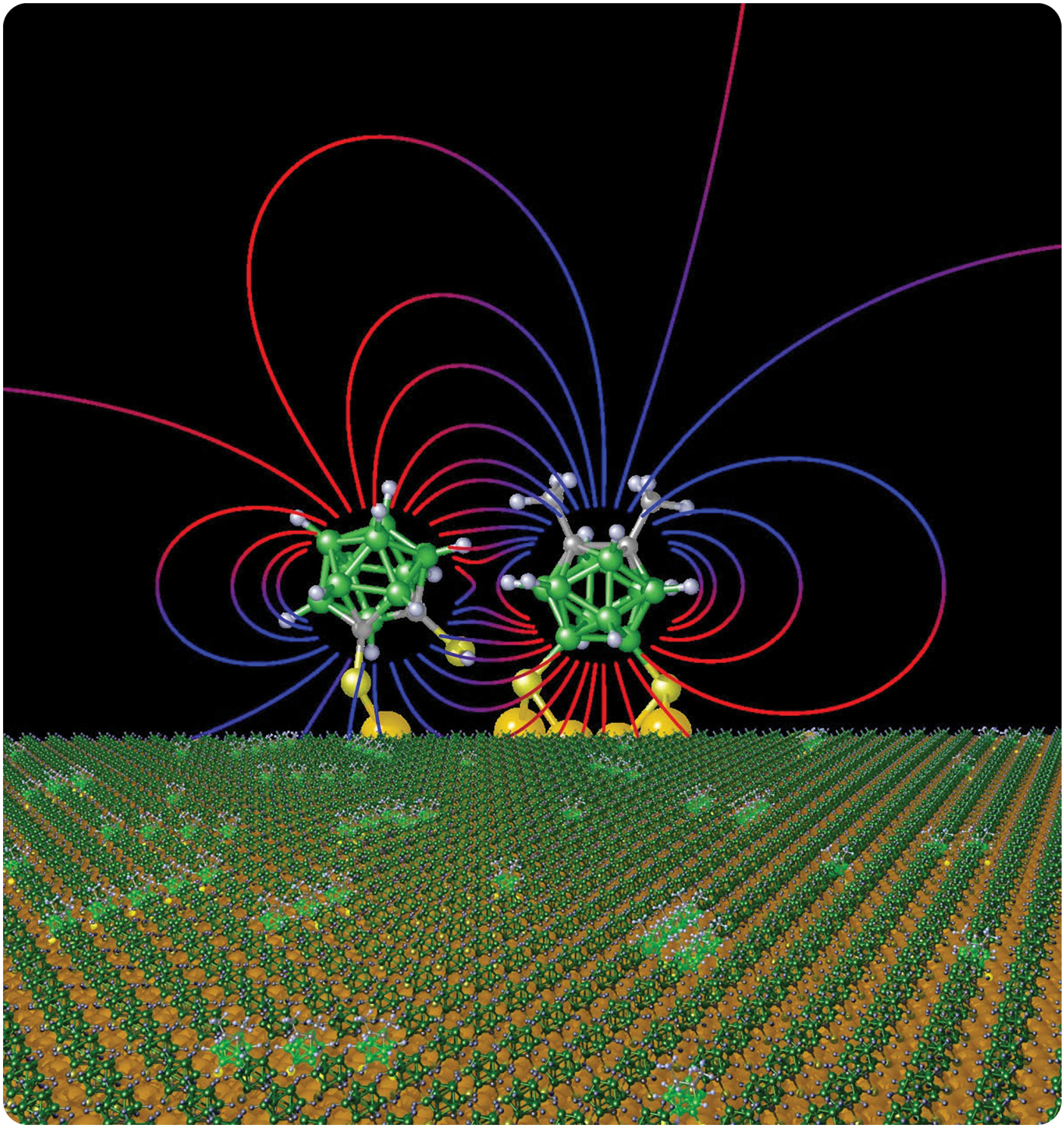

ACS Publications
Most Trusted. Most Cited. Most Read.

www.acs.org

CHEMISTRY OF MATERIALS

pubs.acs.org/cm

Article

Competing Intermolecular and Molecule−Surface Interactions: Dipole−Dipole-Driven Patterns in Mixed Carborane Self-Assembled Monolayers

Katherine E. White, Erin M. Avery, Edison Cummings, Zixiang Hong, Jens Langecker, Aliaksei Vetushka, Michal Dušek, Jan Macháček, Jakub Višnák, Jan Endres, Zdeněk Bastl, Ersen Mete,* Anastassia N. Alexandrova,* Tomáš Baše,* and Paul S. Weiss*

Cite This: *Chem. Mater.* 2024, 36, 2085−2095

Read Online

ACCESS | Metrics & More | Article Recommendations | Supporting Information

ABSTRACT: Carboranedithiol isomers adsorbing with opposite orientations of their dipoles on surfaces are self-assembled together to form mixed monolayers where both lateral dipole−dipole and lateral thiol−thiolate (S−H···S) interactions provide enhanced stability over single-component monolayers. We demonstrate the first instance of the ability to map individual isomers in a mixed monolayer using the model system carboranedithiols on Au{111}. The addition of methyl groups to one isomer provides both an enhanced dipole moment and extra apparent height for differentiation via scanning tunneling microscopy (STM). Associated computational investigations rationalize favorable interactions of mixed pairs and the associated stability changes that arise from these interactions. Both STM images and Monte Carlo simulations yield similarly structured mixed monolayers, where approximately 10% of the molecules have reversed dipole moment orientations but no direct chemical attachment to the surface, leading to homogeneous monolayers with no apparent phase separation. Deprotonating the thiols by depositing the molecules under basic conditions eliminates the lateral S−H···S interactions while accentuating the dipole−dipole forces. The molecular system investigated is composed of isomeric molecules with opposite orientations of dipoles and identical surface packing, which enables the mapping of individual molecules within the mixed monolayers and enables analyses of the contributions of the relatively weak lateral interactions to the overall stability of the assemblies.

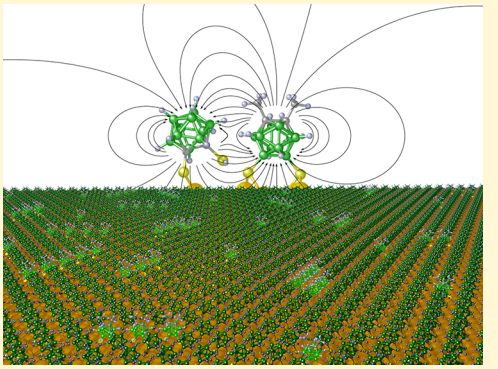

INTRODUCTION

Self-assembled monolayers (SAMs) form ordered two-dimensional (2D) arrays via the adsorption of a headgroup onto a surface and lateral intermolecular interactions.[1,2] These SAMs provide frameworks for studying intermolecular forces in controlled environments.[3−7] The structures and properties of self-assembled materials are influenced by packing interactions similar to those observed in single crystals, where they are commonly referred to as packing forces.[8−11] Generally, it is these interactions that underlie the differences between the properties of single molecules versus ordered arrays of molecules in two or three dimensions.[12] Our previous studies demonstrated that carboranethiols are a natural choice for investigating surface properties given their rigid, regular, and consistent packing structures, tunable surface properties, and applications in electronics and thermal control.[13−19] Previous work investigated the roles of dipoles in self-assembly, but until now it has been difficult to map different isomers with scanning tunneling microscopy (STM) within mixed monolayers as we demonstrate in this study.[18,20−23]

In complex structures, one typically analyzes strong interactions first and to elucidate their roles in self-assembly, be they the supramolecular frameworks of molecules in single crystals or the geometrical surface patterns of 2D arrays of molecules immobilized on surfaces. In the latter systems, anchoring thiol groups strongly interact with the surface and limit the molecules by orienting them in specific ways, thus exposing them to a variety of lateral interactions.[14,24] van der Waals interactions are relatively strong lateral forces, which reflect molecular geometry and space requirements, leading to specific surface patterns.[18,25,26] Any material's structure and function are thus predetermined by competing forces that play active roles during adsorption and the self-assembly process. Understanding these interactions is essential for designing new

Received: December 16, 2023
Revised: January 17, 2024
Accepted: January 18, 2024
Published: February 8, 2024

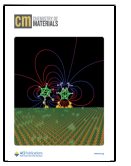

materials of the desired structure and properties. Other groups have studied the interplay between hydrogen bonding and van der Waals interactions in aromatic monolayers, but here, we investigate a different pair: dipole−dipole forces and lateral hydrogen interactions of thiol/thiolate anchoring groups.[27,28]

We use tailored carboranedithiol-based systems, originally introduced and developed for SAMs,[14,29,30] to explore 2D self-organized structures by changing only the properties that we wish to investigate through cage dipole orientation and magnitude while keeping the SAM geometry and bonding scheme identical. In comparison, the common systems of alkyl and aromatic thiols are ill-suited for these purposes, as changes in the dipole moments in organic molecules are usually associated with significant changes in the molecular structures and/or changes in steric requirements.[20,31−33] Here, we build on the significant advantages of the carborane molecular systems to substitute certain fractions of molecules in the respective SAMs with those of different electron density distributions, without changing the surface geometrical patterns.[7,15,17] Such systems have the potential to reveal the effects of different dipole orientations and magnitudes of the molecules on their closest neighbors and beyond and to elucidate the existence of dipole-driven patterns within geometrical molecular arrangements.

RESULTS AND DISCUSSION

The key step necessary in these efforts was to develop the means to differentiate and to identify individual isomers within mixed SAMs to enable molecular mapping. We previously investigated the binding modes of 9,12-$(SH)_2$-1,2-$C_2B_{10}H_8$ (**O9,12**) and 1,2-$(SH)_2$-1,2-$C_2B_{10}H_8$ (**O1,2**) via STM, scanning probe spectroscopic imaging, and lower resolution surface-sensitive techniques. These molecules provide templates to investigate the roles of dipoles and lateral interactions in SAMs, as they have oppositely oriented dipoles, but identical packing structures, with nearest-neighbor spacings of 7.6 Å.[14] The two isomers are practically indistinguishable in STM images under ambient conditions when codeposited in SAMs, making the mapping of individual isomers difficult. To solve this problem, we have increased the contrast by labeling **O9,12** molecules with two methyl substituents on the carbon atoms of the carborane backbone. All three molecules, with their abbreviations and their complete chemical formulas, are depicted in Figure 1. Once assembled on Au{111} surfaces, this dimethyl derivatization changes only the longitudinal space requirement of the parental **O9,12** molecule, i.e., potentially increases the apparent height of these molecules in STM images, while maintaining lateral spacing requirements without disrupting the lateral molecular packing, enabling successful assignment of individual molecules based solely on apparent height, as observed via STM.

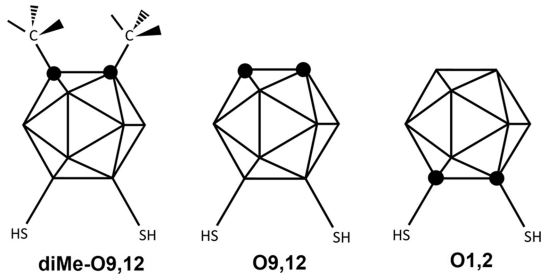

Figure 1. Schematic representation of carboranedithiols: **diMe-O9,12** = 9,12-$(HS)_2$-1,2-$(CH_3)_2$-1,2-$C_2B_{10}H_8$, **O9,12** = 9,12-$(HS)_2$-1,2-$C_2B_{10}H_{10}$, and **O1,2** = 1,2-$(HS)_2$-1,2-$C_2B_{10}H_{10}$. Hydrogen atoms at the vertices of the clusters are omitted for clarity.

Structural and Electronic Properties of diMe-O9,12 (1,2-$(Me)_2$-9,12-$(HS)_2$-1,2-$C_2B_{10}H_8$). Several methods, including computational and X-ray structural analyses, were used to investigate the structure of the dimethyl-labeled derivative, **diMe-O9,12**, and its differences compared to the parent molecule **O9,12** (9,12-$(HS)_2$-1,2-$C_2B_{10}H_{10}$). *Ortho*-carborane, **O9,12**, and the dimethylated derivative of **O9,12**, i.e., **diMe-O9,12**, each have a 2-fold symmetry axis. The thiol groups of **O9,12** form a bridging intramolecular hydrogen bond −S−*H*···*S*(H)−, shown in Figure 2, that is absent in **O1,2**. Attaching thiol (−SH) and methyl ($-CH_3$) groups to the *ortho*-carborane skeleton leads to generally increased interatomic distances between the skeletal atoms. While these changes have an experimentally proven effect on decreasing the thermal rearrangement temperature of the carborane skeleton from *ortho* to *meta* to *para* isomers,[34] they are too subtle to have significant effects on the geometries of the 2D monomolecular assemblies of these molecules on flat Au{111} surfaces, where they retain the nearest neighbor distances of ca. 7.6 Å.[14] Selected structural parameters, obtained experimentally from the single-crystal X-ray diffraction and also computationally (both available in the Supporting Information), of **diMe-O9,12** are presented in Table S2 and sketched in Figure S3. In addition, a side view and a top view of the space-filling computationally optimized model of the molecule are shown. The top view is compared to a circle representing the experimental surface area occupied by one molecule on the surface. The orientations of both methyl groups are longitudinal, protruding above the rigid cages in monolayers, and thus serve as suitable labels of **O9,12** molecules in mixed SAMs with the **O1,2** isomer. We note that both methyl groups, attached to adjacent carbon atoms, are so close to one another that they can potentially rotate only as cog-wheels.[35] The positive inductive effect of the methyl groups further increases the dipole moment from ∼5.5 D of the parent compound **O9,12** to 7.1 D, which makes this derivative exhibit potentially stronger lateral dipole−dipole interactions compared to its nonlabeled analogue.[36]

Supramolecular Structures. Supramolecular structures of thiolated carboranes are usually dominated by hydrogen bonds between the respective thiol groups and CH vertices of the carborane cage(s).[34,37,38] In the case of **diMe-O9,12**, in which the relatively acidic hydrogen atoms at the CH vertices are replaced with methyl groups, it is the relatively strong dipole moment of the molecule, together with its molecular geometry, that leads to a specific single-crystal supramolecular arrangement. This structure consists of separated layers of molecules without any short contacts or hydrogen bonds connecting the layers. Interestingly, all molecules within one layer are arranged with their 2-fold symmetry axes perpendicular to the plane of the layer and in rows with alternating dipole moments. Figure 2 shows the "layered" supramolecular structure with alternating orientations of molecules and thereby with their alternating dipole moments within the layer as well. In Monte Carlo-simulated annealing, the orientations of molecules within a monolayer show dipole moments oriented normal to the surface plane and either up or down, in agreement with the experimentally determined single-crystal arrangement. The molecules with alternating dipole orientations, as observed in

https://doi.org/10.1021/acs.chemmater.3c03210
Chem. Mater. 2024, 36, 2085−2095

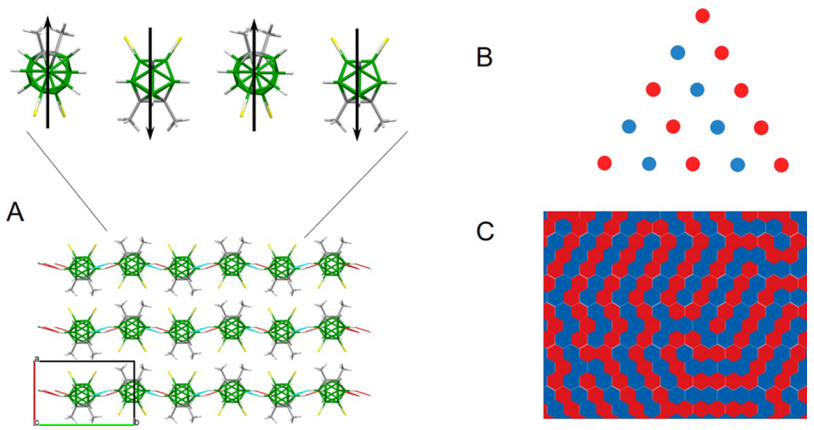

Figure 2. Layered supramolecular arrangement of molecules in a single crystal. (A) (Bottom) Three layers only with short contacts within each layer depicted and (top) four molecules showing an alternating dipole−dipole driven arrangement within one layer. (B) Top view of a fraction of 15 molecules from one layer with either a red or blue background to demonstrate the alternating dipole moment orientation. (C) One observed arrangement from the simulations of dipoles in a 2D layer with only two possible orientations, up or down, is shown as red and blue, respectively.

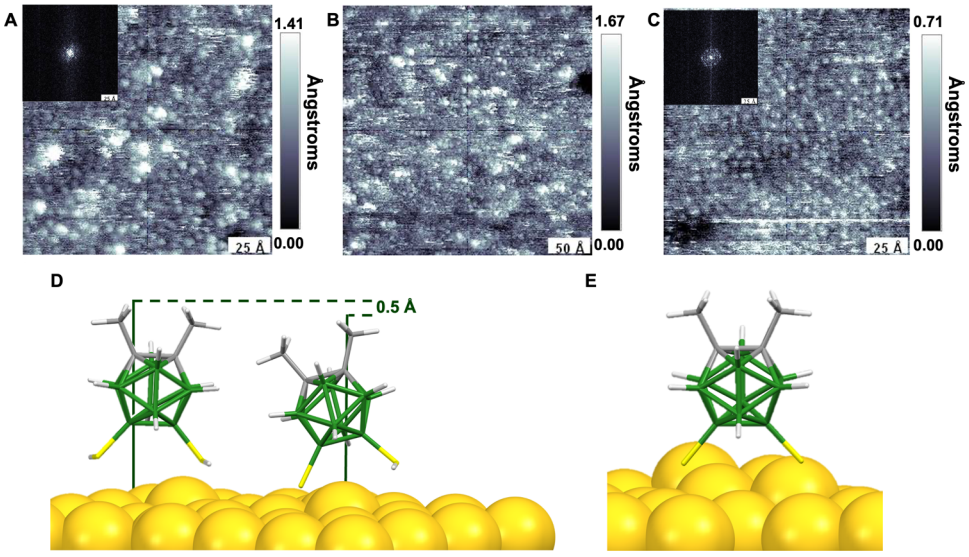

Figure 3. (A−C) Scanning tunneling microscope (STM) images of a pristine **diMe-O9,12** SAM deposited (A, B) under neutral (V_{sample} = −0.1 V, $I_{tunneling}$ = 75 pA, T = 298 K) and (C) basic (V_{sample} = −0.1 V, $I_{tunneling}$ = 100 pA, T = 298 K) conditions on Au{111} at two different resolutions. Insets depict fast Fourier transforms (FFTs) that indicate hexagonally close-packed arrangements with nearest-neighbor spacings of 7.6 ± 0.5 Å. (D) Schematic depiction of two distinct, computationally optimized binding modes, indicating the apparent height difference of 0.5 Å observed under neutral deposition conditions. (E) Computationally optimized geometry of the dithiolate binding mode achieved by depositing molecules under basic conditions.[14]

single crystals, are arranged in infinite parallel lines, while in the Monte Carlo simulated arrangements, the lines of molecules oriented either up or down exhibit random changes as they propagate across the plane. The figure shows one of many arrangements observed in the Monte Carlo simulations.

Scanning Tunneling Microscopy Measurements of Pristine diMe-O9,12 Self-Assembled Monolayers on Au{111}. Monolayers of **diMe-O9,12** molecules were assembled on Au{111}/mica substrates under two different experimental conditions: neutral pH, from EtOH solution; and basic pH, from EtOH solution with equimolar amounts of sodium hydroxide to deprotonate both SH groups prior to their surface adsorption. Both deposition conditions lead to arrays of molecules with identical hexagonal surface arrangements and nearest neighbor distances of 7.6 ± 0.5 Å. Under neutral conditions, STM imaging revealed ca. 10% of molecules appearing to protrude from the monolayer surface (Figure 3A, B). Previous measurements of the parent **O9,12** SAM showed almost no protruding molecules, ∼98 ± 1% of molecules were identified as monovalent (with only one thiol group deprotonated) on the surface, and 2 ± 1% of molecules being adsorbed as divalent (both sulfhydryl groups deprotonated as thiolates).[14] Notably, there was a lack of molecules adsorbing as zerovalent with both thiols still intact. The greater dipole moment of **diMe-O9,12** compared to **O9,12** manifests as the even weaker acidity of the sulfhydryl groups, suggesting that the **diMe-O9,12** molecules might also adsorb as dithiols without deprotonation, as shown in Figure 3D (on the left). Deposition of **diMe-O9,12** under basic conditions, serving in this case also as a comparative reference sample, leads to hexagonally packed SAMs with no apparent protrusions standing out, as shown in Figure 3C, and with the calculated optimized geometry presented in Figure 3E.

https://doi.org/10.1021/acs.chemmater.3c03210
Chem. Mater. 2024, 36, 2085−2095

Previously, we reported on the differences in the apparent heights of adsorbed molecules of **O1,2** and **O9,12** in their SAMs, and we analyzed the inverted contrast in STM images for **O9,12** SAMs in which molecules bound as divalent appeared more protruding from the surface despite having their geometrical height lower compared to the monovalent bound molecules.[14] This particular aspect of adsorption is investigated further and verified in this study by demonstrating that molecules of diMe-**O9,12**, being weaker acids than **O9,12** (i.e., showing even lower tendency to lose the sulfhydryl protons), adsorb predominantly as zerovalent (physisorbed dithiols) and appear less protruding in STM images of the respective SAMs, consistent with simulated STM images of all three binding modes of **diMe-O9,12** molecules presented in Figure 3D,E. The **diMe-O9,12** system therefore presents a novel binding mode not observed previously in carboranedithiol monolayers: complete physisorption with both thiols still protonated.

The presence of both thiol- and thiolate-adsorbed moieties in the SAM was further shown by X-ray photoelectron spectra (XPS) with the respective binding energy values of S 2p photoelectrons at 161.7 ± 0.1 and 163.0 ± 0.1 eV, as shown in Table 1. The latter value is the same, within experimental error,

Table 1. Measured Core-Level Binding Energies in eV and Full-Width Half Maxima (in Parentheses) for Au Films Modified with diMe-O9,12 and for a Solid Crystalline Sample of O9,12 for Comparison

sample	**O9,12** (crystalline sample)	**diMe-O9,12** SAM/Au
stoichiometry	$B_{10}S_{2.1}C_{2.1}$	$B_{10}S_{2.2}C_{5.6}$
S $2p_{3/2}$	162.9 (2.2)	161.7 (1.1), 163.0 (1.1)
B 1s	189.7 (2.5)	189.6 (1.8)
C 1s	286.6 (2.3)	285.3 (1.5), 286.7 (1.6)

as for the crystalline **O9,12** derivative, indicating the existence of thiol on the gold surface and validating the presence of both zerovalent and monovalent binding modes. The relatively low binding energy of S 2p on gold in the **diMe-O9,12** is consistent with the electron-donating nature of B−S−H-bonded carboranethiols as well as previous reports.[14,29,37]

Lateral Molecular Interactions Analysis in Mixed Self-Assembled Monolayers. Lateral interactions in SAMs cover those of carboranes' backbones as well as interactions of their anchoring groups. To understand stabilizing or destabilizing effects, we have carried out calculations of isomeric pairs of molecules in a vacuum and also adsorbed on gold surfaces.

Pristine and Mixed Pairs of Free Molecules. *Thiol-Anchoring Groups and Their SH···S(H) Intermolecular Interactions.* Understanding experimental results obtained with mixed monolayers of **O1,2** and **O9,12** (or its dimethyl-labeled analog: **diMeO9,12**) requires analyzing their lateral intermolecular interactions. To disentangle these interactions that take place in the respective 2D arrays, we first computationally investigated pairs of free molecules (both pristine and mixed) by copying their dipole moment orientations and nearest neighbor distances from arrays on gold surfaces but omitting their interactions with the gold surface in our first approximation, thus focusing purely on lateral interactions within the respective pairs. All three species and their respective SAMs have several common features: (1) similar, or practically identical, molecular geometries with a two-fold symmetry axis, as shown and discussed above (Figure 1); (2) assembly into hexagonal close-packed patterns on gold surfaces (Figure 3) with identical nearest neighbor distances; (3) relatively strong dipole moments, with by far the strongest in the case of **diMe-O9,12** molecule at 7.1 D; and (4) sulfhydryl group acidities that manifest in strong electron-donating (**O9,12** and **diMe-O9,12**) and withdrawing (**O1,2**) effects, depending on to which vertices the SH groups are attached.

We used scanning Kelvin probe force microscopy to investigate surface potential changes as a measure of dipole moment magnitude and orientation of the molecules on the surface.[7] In agreement with the orientation and magnitudes of the dipoles, the **O1,2** SAM significantly decreases the surface potential of the metal substrate, while **O9,12** increases the value, and **diMe-O9,12** increases it even more as shown in Figure 4. The surface potential shifts are consistent with the

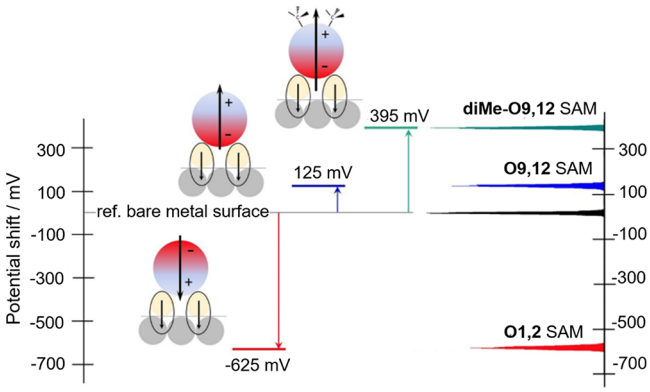

Figure 4. Surface potential shifts caused by SAMs of **O1,2**, **O9,12**, and **diMe-O9,12** with the respective histograms (on the right) showing narrow distributions of values as analyzed by using scanning KPFM.

effects of the orientation and the relative dipole strength of **diMe-O9,12** and the respective SAM. See Figure S10 in the Supporting Information for more details.

Two molecules positioned as close to each other as found on gold surfaces, ca. 7.6 Å, can interact through their molecular backbones by their dipole−dipole moments and through structural elements such as their surface-anchoring thiol groups.[7,17] The latter can form intramolecular as well as intermolecular hydrogen bonds. To evaluate these lateral interactions and estimate their contributions to how homogeneously the molecules distribute in a SAM, we carried out calculations, the results of which are depicted in Figure 5 (with all of the results summarized and presented in Table S4 and Figure S12). These results demonstrate significant differences in the strengths of mutual interactions in different molecular pairs.

The interactions between two carboranedithiol molecules are dominated by those between their thiol groups, specifically between the thiol hydrogen of one molecule and the sulfur of a neighbor. This intermolecular interaction is stronger and more stabilizing in the case of two molecules of **O9,12** than in two molecules of **O1,2**. However, by far, the strongest case is a mixed pair with the interaction between the hydrogen of a thiol group bound to a skeletal carbon atom (C−S−H) of **O1,2** and the sulfur bound to a boron atom (B−S) in **O9,12**. The opposite orientation of the -SH···S- hydrogen interaction, i.e., from the hydrogen of a boron-bound thiol group (B−S−H) of

https://doi.org/10.1021/acs.chemmater.3c03210
Chem. Mater. 2024, 36, 2085−2095

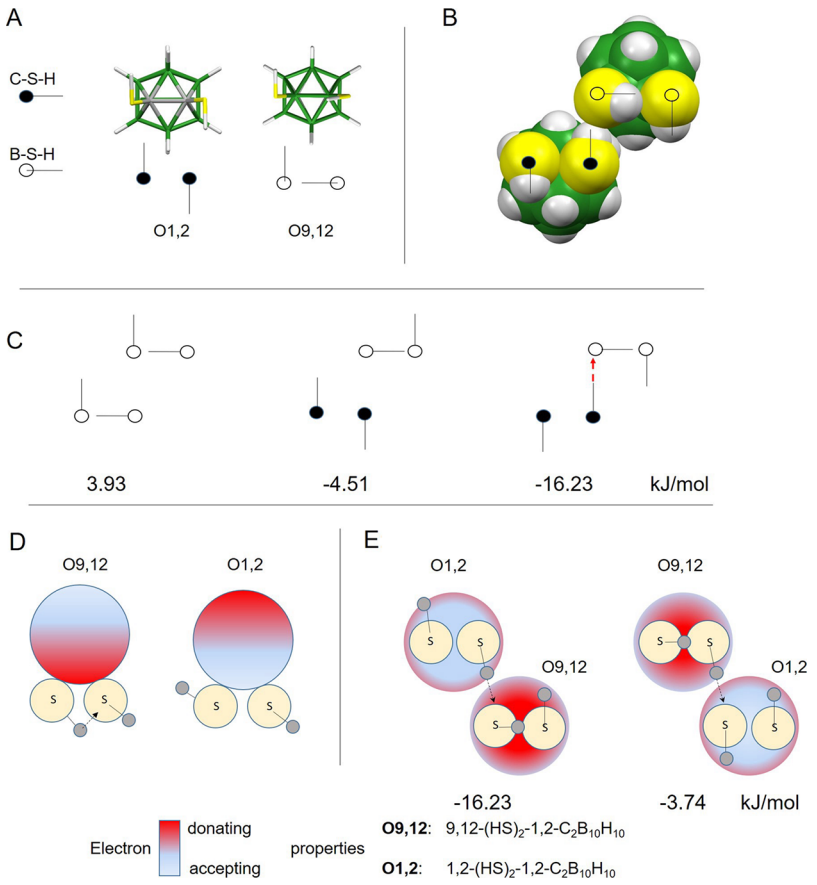

Figure 5. (A) Computationally optimized isomeric carboranedithiols of **O1,2** and **O9,12** with sulfhydryl group conformations in their global energy minima. (B) Space-filling model of a pair of molecules of **O1,2** and **O9,12** exhibiting intermolecular C-*SH*···*S*(H)B interaction. (C) Schematic representation of three mixed pairs of **O1,2** and **O9,12** showing for simplicity only the sulfhydryl groups and their particular conformations. The pairs on the left and in the middle are calculated with no intermolecular *SH*···*S* interactions, while the one on the right does include this interaction. The full black dots represent sulfur atoms attached to the carbon vertices of the carborane clusters, the hollow dots represent sulfur atoms attached to the boron vertices of the carborane clusters. (D) Side view schematic of both isomers showing electron-donating (red) and -accepting (light blue) properties of the carborane scaffold with the respective dipole moment orientation. (E) Bottom view of two mixed pairs with −*SH*···*S*− interactions.

Table 2. Calculated Adsorption and Interaction Energies in eV of Pairs of Molecules on a Au{111} (7 × 4) Slab[a]

pair: dithiol1-dithiol2	O1,2-O1,2	O9,12-O9,12	O1,2-O9,12	O9,12-O1,2
$E_{\text{pair adsorption on Au\{111\}}}$	−8.86	−9.11	−8.95	−8.87
$E_{\text{pair interaction on Au\{111\}}}$	−0.11	0.02	−0.22	−0.16

[a]Additional details are provided in the Supporting Information.

O9,12 to a carbon-bound sulfur group (C−S) of **O1,2**, is significantly weaker, as shown in Figure 5e. Correspondingly, the optimized structure of a single free molecule of **O9,12** shows an advantageous intramolecular −*SH*···*S*(H)− hydrogen bond between its thiol groups (Figure S3), while the molecule of **O1,2** does not. These computational results are consistent with the electron-donating effects of the carborane moiety at its skeletal boron positions and electron-accepting effects at the skeletal carbons while simultaneously elucidating these electronic effects' contributions to maximize the distributions of molecules in mixed SAMs.

The advantageous orientation of two dipoles parallel but oppositely oriented dipole moments in mixed pairs of molecules (**O1,2** and **O9,12**) are significantly more stable compared to their pristine pairs in which dipole moments are also parallel but oriented in the same direction.[7] Moreover, in the pairs of **O9,12** molecules calculated in conformations unsuitable for (i.e., without) intermolecular hydrogen bonding (Figure 5C) to eliminate their stabilizing effects, the interactions between the two molecules were found to be repulsive, which we attribute to destabilizing parallel interactions of their relatively strong dipole moments.

In mixed pairs, these results demonstrate the synergic effects of two types of lateral interactions found in the single crystals of **diMe-O9,12**: (1) the molecules' anchoring SH groups and (2) the molecular backbones via their dipole moments, with both contributions governing arrangements and leading to greater stability of mixed pairs. In this case, we see potentially competing intermolecular forces that interfere constructively with increased stability in a lower energy conformation.

Pristine and Mixed Pairs of Molecules on Au{111}. The previously discussed analyses of intermolecular interactions in free pairs of molecules, oriented in a fashion similar to that on gold surfaces, do not, at a first approximation, cover

https://doi.org/10.1021/acs.chemmater.3c03210
Chem. Mater. 2024, 36, 2085−2095

the interactions with gold surfaces. Therefore, calculations with several pairs of molecules adsorbed on 7 × 4 gold slabs were carried out to investigate the effects of surface adsorption. Considering the adsorption energies summarized in Table 2, a pair of **O9,12** molecules shows the greatest stability (adsorption energy of −9.11 eV) followed by the two pairs of mixed molecules of **O1,2** and **O9,12**, and the least stable pair is represented by two molecules of **O1,2** on gold surfaces. This particular order results from the stabilizing effects of B−S−Au bonds, which are significantly more stable than the respective C−S−Au bonds. The ratio of B−S−Au to C−S−Au bonds in the investigated pairs follows the trend observed in the adsorption energies: 3:0 in a pair of two **O9,12** molecules (Figure 6B); 2:1 in a mixed pair of **O1,2** and **O9,12** (Figure 6C); 1:2 in a pair of **O9,12** and **O1,2** (Figure 6D); and 0:3 in a pair of two **O1,2** molecules (Figure 6A). However, the adsorption energy value does not show the stabilizing or destabilizing effects of lateral interactions, which are more important for understanding the 2D patterns of SAMs. To assess the lateral forces between molecules in the respective pairs, we calculated the pair interaction energies using the following equation:

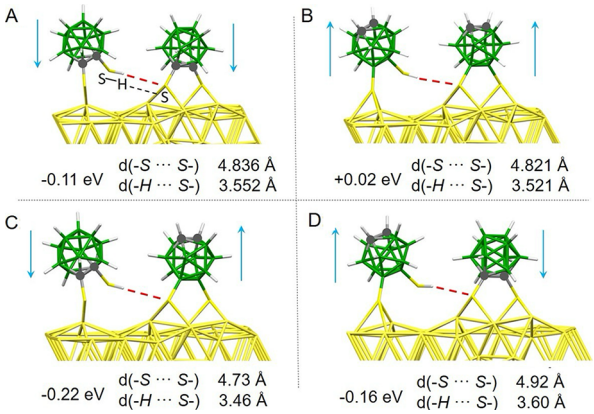

Figure 6. Computationally optimized pairs of isomeric carboranedithiols, **O1,2** and **O9,12**, on a gold surface with −S−H···S− hydrogen interactions indicated. (A) An **O1,2** and **O1,2** pair, (B) an **O9,12** and **O9,12** pair, (C) an **O1,2** and **O9,12** mixed pair, and (D) an **O9,12** and **O1,2** mixed pair. The lateral pair interaction energy is shown in eV. Larger gray dots indicate the positions of carbon atoms in the carborane cage backbones.

$$E_{\text{pair interaction on Au\{111\}}} = E_{\text{pair on Au\{111\}}} - E_{\text{dithiol 1 on Au\{111\}}} - E_{\text{dithiol 2 on Au\{111\}}} + E_{\text{Au\{111\}}}$$

and sorted the pairs accordingly. These results cover both the lateral hydrogen-bonding interactions of anchoring groups influenced differently by carborane backbones via their electron-withdrawing and electron-accepting properties as well as direct dipole−dipole interactions of the molecular backbones. The mixed pairs of molecules **O1,2** and **O9,12** (Figure 6C) show the greatest stabilizing effects with the pair interaction energy of −0.22 eV followed by the second mixed pair of molecules **O9,12** and **O1,2**, then the pair of molecules of **O1,2**, and the least stable, a pair of two molecules of **O9,12**, which represent two molecules with strong dipole moments aligned unfavorably in the same direction. These results follow the trend discussed above for computational investigations of free pairs of molecules.

As further observed in additional experimental STM results, Figure S9 in the Supporting Information, the mixed SAMs of **O1,2** and **O9,12** (or the **diMe-O9,12**) deposited under neutral conditions lead to images where it is difficult to assign the individual molecules due to their distinct binding modes. Therefore, in another experiment, we focused on mixed SAMs resulting from coadsorption of both **O1,2** and **diMe-O9,12** in a 1:9 ratio as two molecules, providing the greatest possible apparent height differences in STM images after deposition under basic conditions to maximize the fractions of molecules that adsorb in the divalent mode only. In addition, basic deposition avoids any possibility for interactions between the anchoring groups via their hydrogen −*SH*···*S*(H)− bonds due to prior deprotonation of the SH groups.

As a result of both labeling **O9,12** molecules with two methyl groups as well as the basic deposition conditions, we assign the more protruding molecules in the experimental STM images of the mixed SAMs of **diMe-O9,12** and **O1,2**, Figure 7, to the molecules of **diMe-O9,12** distributed in the monolayer. The apparent height of **diMe-O9,12** is 0.7 Å higher than **O1,2**, as illustrated in Figure 7C. While we do not observe in Figure 7A, B the simulated Monte Carlo patterns shown in Figure 7D, importantly, there is no phase separation, as seen in our previous study investigating a carboxylated *para*-carboranethiol in a matrix of unfunctionalized *para*-carborane.[38] The *para*-carboranes that were investigated in a similar molar ratio and the carboxylated molecules formed islands instead of the homogeneous mixtures that we see here. The Monte Carlo simulations take only the dipole−dipole interactions into account. If those forces were the only factor in self-assembly, then **diMe-O9,12** would be perfectly distributed in the matrix of **O1,2** in ideal monolayers, given their oppositely oriented dipoles. As previously discussed in detail, this system also investigates the differences in anchoring group interactions for B−S−H as compared to C−S−H. The combinations of these

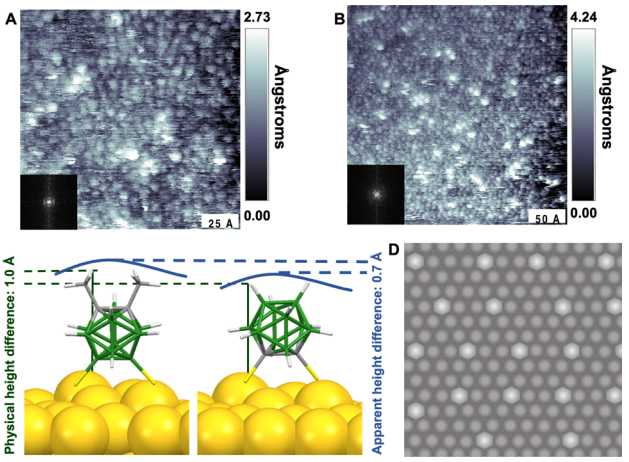

Figure 7. (A, B) Scanning tunneling microscope (STM) images of a mixed **diMe-O9,12** and **O1,2** SAM deposited from a solution with a 9:1 ratio of **diMe-O9,12** to **O1,2** under basic conditions on Au{111}/mica at two different resolutions (V_{sample} = −0.1 V, $I_{\text{tunneling}}$ = 105 pA, and T = 298 K. (C) Schematic of two distinct binding modes with an apparent height difference of 0.7 Å in the STM images. (D) Result of dipole−dipole interaction simulation in a hexagonal field with 10% of molecules having the opposite dipole moment orientation.

https://doi.org/10.1021/acs.chemmater.3c03210
Chem. Mater. 2024, 36, 2085−2095

intermolecular forces lead to our observed experimental results and explain the differences from the Monte Carlo simulations.

CONCLUSIONS AND PROSPECTS

We have addressed the relatively complicated issue of disentangling weak interactions within SAMs, including the importance of dipole−dipole interactions that occur within many molecular self-assembled systems but remain largely unnoticed or hidden behind much stronger interactions. We have designed and characterized a new derivative of 1,2-dicarba-*closo*-dodecaborane-9,12-dithiol (**O9,12**), which was used previously as a constituent of SAMs demonstrating how the thiol group acidity influences its adsorption. The new derivative, 1,2-dimethyl-1,2-dicarba-*closo*-dodecaborane-9,12-dithiol (**diMe-O9,12**), which is a version of its parent molecule labeled with two distal methyl groups, has identical lateral steric requirements in its respective SAMs as the parent, and as its isomeric 1,2-dicarba-*closo*-dodecaborane-1,2-dithiol (**O1,2**). The two methyl groups increase the longitudinal steric demands of the **O9,12** molecule, enabling differentiation from **O1,2** in the STM images. The new derivative has been structurally characterized using single-crystal diffraction analysis, which revealed a supramolecular structure driven by dipole−dipole interactions, fittingly with the large dipole moment of the molecule (7.1 D). When deposited on gold surfaces under neutral conditions, the pristine SAMs of this derivative show that the molecules adsorb 90% in zerovalent mode (i.e., as fully physisorbed dithiols) and 10% in monovalent mode. The molecules adsorbed in the less abundant monovalent mode appear more protruding in STM images, as confirmed by simulations. When deposited under basic conditions, all molecules of the pristine **diMe-O9,12** SAM were adsorbed as divalent (i.e., as fully chemisorbed dithiolate moieties) without any significantly differing apparent heights. In this study, within the focus on lateral interactions within SAMs, we have analyzed two essential contributions: first, hydrogen-bonding interactions between the anchoring SH groups of adjacent molecules and, second, lateral dipole−dipole interactions driven mainly by the carborane backbones. Both interactions increase the stability of mixed SAMs consisting of two components of opposite dipole moment orientation and lead to arrays of molecules with alternating dipoles. Experimentally, codeposition of **O1,2** and **O9,12** (or **diMe-O9,12**) molecules under neutral conditions leads to monolayers with apparent protrusions affected by different binding modes of the individual constituents, which makes it difficult to assign the molecules to each isomer. Narrowing the problem by depositing molecules under basic conditions, thus avoiding the sulfhydryl group interactions, and by codepositing **O1,2** with the labeled **diMe-O9,12** to increase their apparent height differences enables the identification of each molecule within the STM images of the mixed SAMs. Consistent with dipole−dipole interactions in Monte Carlo simulations, the molecules are well separated and homogeneously distributed over the surface within the mixed SAMs.

EXPERIMENTAL SECTION

General Procedures, Chemicals, and Materials. Carboranedithiol derivatives (**O1,2** and **O9,12**) as well as 9,12-bis(methoxymethylthio)-*o*-carborane starting precursor (herein further referred to as CB-MOM) for the synthesis of **diMe-O9,12** were prepared according to the literature.[39] The purity was checked by gas chromatography with mass spectrometry detection (GC-MS) and ^{11}B and ^{1}H NMR spectroscopy. Nuclear magnetic resonance spectroscopy was performed at room temperature on a Varian MercuryPlus at 400 MHz using standard techniques and procedures. Solvents for synthesis (such as tetrahydrofuran, THF) were purchased from Penta a.s. Czech Republic, and additionally dried with sodium in the presence of benzophenone (99.8%, purchased from Sigma-Aldrich) and freshly distilled before experiments. Other solvents were used as received. Solvents for STM experiments were purchased from Sigma-Aldrich and used as received. The NMR spectra were measured in CDCl3 (99.8% D) as received from Eurisotop.

Synthesis of diMe-O9,12. *1,2-Dimethyl-9,12-SMOM-o-carborane.* 0.838 g (2.89 mmol) of CB-MOM were dissolved in 30 mL of dry and freshly distilled THF under nitrogen atmosphere and cooled to 0 °C in an ice−water bath. 2.34 mL (5.85 mmol) of *n*-BuLi (2.5 M solution in hexanes) were added dropwise via syringe. After 5 min, 0.825 g (5.81 mmol) of methyl iodide was added dropwise, still cooling, and stirred overnight at room temperature. The solvent was removed, and the residue was dissolved in diethyl ether and extracted twice with distilled water (30 mL). The solution was dried over anhydrous sodium sulfate and filtered through a layer of silica gel. Removal of the solvent by evaporation on a rotary evaporator gave viscous oil, which slowly solidified. Yield: 1.205 g.

1,2-Dimethyl-9,12-(SH)2-o-carborane, ***diMe-O9,12.*** 0.74 g (2.28 mmol) of 1,2-dimethyl-9,12-SMOM-*o*-carborane were dissolved in 25 mL of acetonitrile/water (4:1). A solution of 1.251 g (4.61 mmol) mercury(II) chloride in 2−3 mL of acetonitrile/water (4:1) was added, and the mixture was stirred for 2 h. White precipitate was collected by filtration and washed with 10 mL of acetonitrile/water (4:1) and 10 mL of water. The solid product was suspended in chloroform and H_2S was bubbled through the suspension while a black precipitate was formed (HgS). The mixture was filtered by using a syringe filter. Evaporation of the solvent gave a white crude product, which was further purified by sublimation under reduced pressure (~10^{-2} mbar) at 120 °C with a yield of 90%.

Monolayer Preparation. Ethanol and NaOH pellets were used as received (Sigma-Aldrich, St. Louis, MO). Au{111}/mica substrates (Keysight Technologies, Santa Rosa, CA) were hydrogen-flame annealed prior to SAM formation with 10 passes at a rate of 0.4 Hz. Monolayers deposited under neutral conditions were prepared by immersion in 1 mM ethanolic solution at room temperature for approximately 24 h. Monolayers deposited under basic conditions were prepared by mixing 0.5 mL of 4 mM NaOH in EtOH and 0.5 mL of 2 mM **O1,2**, **O9,12**, or **diMe-O9,12** and immersing flame-annealed Au{111}/mica substrates at room temperature for 1 h.

EXPERIMENTAL METHODS

Scanning Tunneling Microscopy. Samples for imaging were prepared on Au{111}/mica substrates (Agilent Technologies, Santa Clara, CA), which were hydrogen-flame annealed with 10 passes at a rate of 0.4 Hz prior to monolayer deposition. Ethanol and NaOH pellets were used as received (Sigma-Aldrich, St. Louis, MO). Substrates were placed in a capped vial with 1 mL of a 1 mM solution of the respective isomer or mixture of isomers in ethanol for 24 h for deposition under neutral conditions. Samples deposited under basic conditions were deposited for only 10 min in order to decrease the possibility of degradation. After deposition, samples were cleaned with neat ethanol and dried with a stream of nitrogen gas three times before being loaded into the STM.

All STM measurements were performed with a custom-built Besocke-style with a platinum/iridium tip (80:20) in constant current mode under ambient conditions.[40] Samples were held at a fixed bias (V_{sample} = −0.1 V). The known lattice of the 1-dodecanethiolate SAMs on Au{111} was used for calibration. The STM image analysis was done using MATLAB (Mathworks, Natick, MA) and Gwyddion (http://gwyddion.net/).

X-ray Photoelectron Spectroscopy. The XPS of the samples were measured using a modified ESCA 3 MkII multitechnique spectrometer equipped with a hemispherical electron analyzer operated in fixed transmission mode. Al K_α radiation was used for

https://doi.org/10.1021/acs.chemmater.3c03210
Chem. Mater. 2024, 36, 2085−2095

electron excitation. The binding energy scale was calibrated by using the Au $4f_{7/2}$ (84.0 eV) and Cu $2p_{3/2}$ (932.6 eV) photoemission lines. The pressure in the XPS analysis chamber during spectral acquisition was 6×10^{-9} mbar. The powdered sample was spread on an aluminum surface. The spectra were collected at a takeoff angle of 45° with respect to the macroscopic surface normal. Survey scan spectra and high-resolution spectra of B 1s, C 1s, and S 2p photoelectrons were measured. The spectra were fit after subtraction of Shirley background using the Gaussian−Lorentzian line shape and nonlinear least-squares algorithms (CasaXPS software). Binding energies of the powdered samples were referenced to C 1s peak of adventitious carbon at 284.8 eV. Quantification of the elemental concentrations was accomplished by correcting the photoelectron peak intensities for their cross-sections and for the analyzer transmission function. In calculations, homogeneous compositions of the analyzed samples layer were assumed.

Computational Investigations. *Free Pairs of Molecules.* Quantum chemistry calculations were performed using the NWChem[41] package. The geometries were optimized[42] by means of density functional theory (DFT) with the hybrid exchange−correlation functional PBE0[43,44] using Jensen's double−zeta segmented polarization consistent basis set pcseg-1.[45]

Two molecules of *closo*-dicarbadodecaboranedithiol were placed in positions resembling their arrangements in monolayers on metal surfaces, the (approximate) planes formed by the sulfur atoms and C1, C2, B9, and B12 cage atoms of each molecule set parallel, and the four sulfur atoms situated in one plane perpendicular to those two in the pattern of the monolayer elementary cells. The sulfur atoms from the geometries, as taken from our previous studies, were leveled.[14] The positions of the four sulfur atoms were then fixed, and the positions of all of the other atoms were optimized. Several calculations were performed for each pair (**O1,2** + **O1,2**; **O9,12** + **O9,12**; and **O1,2** + **O9,12**) with different conformations of the thiol hydrogens to determine the configuration with the minimum energy. Then, the energies of each of the molecules of such pairs were calculated separately in the geometries of the molecules in the optimized pairs, with the atoms of the other molecules replaced by ghost atoms to preserve identical basis sets. The energy of interaction between the two molecules was calculated for each pair as the difference between the sum of the energies of the individual molecules and the energy of the pair.

Pairs of Molecules Adsorbed on Gold Surfaces. Theoretical studies, based on DFT, estimated quantifiable characteristics of carboranethiol SAMs on Au{111} consistent with experiments.[46] Following the same framework, dispersion-corrected density functional theory (vdW-DFT) calculations were performed to gain further insight into the adsorption characteristics through atomistic modeling of isomeric carboranidiniols on the gold surface. The projector-augmented wave method was used as implemented in VASP (version 6.3).[47−49] Variational minimization of the ground state energy of each model structure was achieved through plane wave basis expansion of the Kohn−Sham (KS) orbitals up to a 400 eV cutoff. The exchange−correlation (XC) effects were taken into account by employing the contemporary Strongly Constrained and Appropriately Normed (SCAN) functional, which was proposed to heal numerical instabilities of the standard functionals of generalized gradient approximation by imposing additional constraints to reproduce accurate reference values.[50] Moreover, the intermolecular interactions within SAMs require consideration of the dispersive corrections. For this purpose, we incorporated revised Vydrov-van Voorhis (rVV10) nonlocal correlation energies as complemented in the modern SCAN + rVV10 functional.[51,52] This method not only gives a better estimation of the lattice constant of gold among standard and van der Waals (vdW)—supplemented DFT functionals but also improves the description of metal−organic interface properties relative to benchmarked vdW-DFT functionals in comparison with the experiments.[52−55]

Periodic boundary conditions (PBC) were assumed, and the (111) surface of gold was represented with four-layer slab models, which were built by replication of the bulk unit cell and then by termination through (111) planes to expose top and bottom faces. Matched and mixed pairs of **O1,2** and **O9,12** carborane dithiols were considered on a (7 × 4) slab (with X- and Y-dimensions of 19.20 and 10.97 Å, respectively), and **diMe-O9,12** SAMs were modeled using a (4 × 4) slab (with two distinct binding modes, as shown in Figure 6D). Each computational supercell contains one of the slab models with one or more molecular adsorbates and a vacuum region with a height of at least 12 Å to avoid unphysical interactions between the periodic images of the slabs. We report the minimum energy geometries of molecules on the surface, which were determined by tracing all of the probable adsorption sites. The geometry optimizations were achieved by imposing a convergence criterion based on the minimization of the Hellmann−Feynman forces on each atom to be smaller than 10^{-2} eV/Å. The Brillouin zone integrations were carried out over Γ-centered 6 × 6 × 1 and 3 × 6 × 1 *k*-point samplings for the (4 × 4) and (7 × 4) surface cells, respectively. Technically, occupation of the electronic states at the Fermi energy (E_F) was smeared by using the Methfessel−Paxton (MP) scheme with a parameter of 0.1 eV. The dipole corrections were also included in the polar slab calculations.

The lateral pair interactions between matched and mixed isomeric carboranedithiols of **O1,2** and **O9,12** on Au{111} (including −S-H···S− interactions, as shown in Figure 4) were calculated using the (7 × 4) slab model with the expression:

$$E_{\text{pairint}} = E_{\text{AB/Au}\{111\}} + E_{\text{Au}\{111\}} - E_{\text{A/Au}\{111\}} - E_{\text{B/Au}\{111\}}$$

where the first and the second molecules are labeled as A and B, respectively. $E_{\text{AB/Au}\{111\}}$ is the total supercell energy of the slab with the pair of adsorbates, $E_{\text{Au}\{111\}}$ is the energy of the clean slab. $E_{\text{A/Au}\{111\}}$ and $E_{\text{B/Au}\{111\}}$ are the energies of the gold slabs with the other adsorbate molecule of the pair removed.

Computationally Simulated Scanning Tunneling Microscope Images. Two Au{111} surfaces were modeled, with a 4 × 4 × 4 atom surface to study individual carboranes and a 4 × 7 × 4 atom surface to study two interacting carboranes, using a [10.97500,0,0] × [5.48750,9.50463,0] × [0,0,28.50000] $Å^3$ supercell and a [19.20500,0,0] × [5.48750,9.50463,0] × [0,0,24.50000] $Å^3$ supercell, respectively, with four layers along *z*. The bottom two layers were fixed during optimization for both cases. To be consistent with the experiment, the calculated lattice constant for Au was chosen to be 2.95 Å. To prepare the STM images and the charge density plots, we continued using a 5 × 5 × 1 Monkhorst−Pack *k*-point grid. An energy range of −0.1 eV to E_F was used in the partial charge density calculations. Then, the STM images were simulated by using the Tersoff−Hamann approximation and the program p4vasp, with a constant tip height of 21.3 Å.

Monte Carlo Simulations. We used simulated annealing to explore the optimal distribution of dipoles with different orientations. Simulations were performed on 2D hexagonal lattices with a lattice parameter a = 7.6 Å; 2D PBCs were used. Dipole moments were set to 3.6 and 5.7 D, respectively, taken from the calculated dipole moments of the free thiols **O1,2** and **O9,12**; for comparison, the same set of simulations was performed with opposite dipoles of identical magnitude 4.5 *D*, the dipole moment of the parent *ortho*-carborane.

The ratio of dipoles with opposite orientation was fixed during each simulation, and dipoles were randomly distributed in the lattice at the start of the simulation. In each simulation step, we randomly chose two dipoles with opposite orientations and switched their positions in the lattice. We determined the energy difference, the ΔE, connected with this change. When the energy difference ΔE was negative, a new state was automatically accepted. In the case of positive ΔE, the probability of acceptance of this new state was

$$\exp\left(\frac{-\Delta E}{K_B T}\right)$$

where k_B is the Boltzmann constant and T is the simulation temperature. The temperature was progressively decreased from an initial value toward zero. The starting temperature was set to 1000 K, at which almost all new states were accepted. After 200,000 accepted simulation steps, the temperature was multiplied by 0.8, and the

https://doi.org/10.1021/acs.chemmater.3c03210
Chem. Mater. 2024, 36, 2085−2095

simulation continued. A complementary limit of 400,000 attempted steps was applied for lower temperatures, as the ratio of the accepted steps was reduced. The simulation was stopped after 30 temperature reductions, at a temperature of 1.24 K, sufficiently close to zero, such that only changes lowering the system energy were accepted. Because of long-range dipole interactions and the periodicity of the simulation lattice, Ewald summation for confined geometry was used to determine the energy change.[56]

■ ASSOCIATED CONTENT

Supporting Information

The Supporting Information is available free of charge at https://pubs.acs.org/doi/10.1021/acs.chemmater.3c03210.

Nuclear magnetic resonance data; crystallographic information; supramolecular structures; mass spectrometry analyses; infrared spectra; additional STM results; and additional computation results, including for free molecules and pairs of molecules, adsorbed molecules, simulated STM images, and Monte Carlo simulations (PDF)

■ AUTHOR INFORMATION

Corresponding Authors

Ersen Mete − *Department of Physics, Balikesir University, Balikesir 10145, Turkey;* orcid.org/0000-0002-0916-5616; Email: emete@balikesir.edu.tr

Anastassia N. Alexandrova − *Department of Chemistry and Biochemistry, California NanoSystems Institute, and Department of Materials Science and Engineering, University of California, Los Angeles, Los Angeles, California 90095, United States;* orcid.org/0000-0002-3003-1911; Email: ana@chem.ucla.edu

Tomáš Baše − *Department of Chemistry and Biochemistry and California NanoSystems Institute, University of California, Los Angeles, Los Angeles, California 90095, United States; The Czech Academy of Sciences, Institute of Inorganic Chemistry, Husinec-Rez 250 68, Czech Republic;* orcid.org/0000-0003-2533-8705; Email: tbase@iic.cas.cz

Paul S. Weiss − *Department of Chemistry and Biochemistry, Department of Bioengineering, Department of Materials Science and Engineering, and California NanoSystems Institute, University of California, Los Angeles, Los Angeles, California 90095, United States;* orcid.org/0000-0001-5527-6248; Email: psw@cnsi.ucla.edu

Authors

Katherine E. White − *Department of Chemistry and Biochemistry and California NanoSystems Institute, University of California, Los Angeles, Los Angeles, California 90095, United States;* orcid.org/0000-0001-5050-6024

Erin M. Avery − *Department of Chemistry and Biochemistry and California NanoSystems Institute, University of California, Los Angeles, Los Angeles, California 90095, United States;* orcid.org/0000-0002-6361-6967

Edison Cummings − *Department of Chemistry and Biochemistry, University of California, Los Angeles, Los Angeles, California 90095, United States*

Zixiang Hong − *Department of Chemistry and Biochemistry, University of California, Los Angeles, Los Angeles, California 90095, United States*

Jens Langecker − *The Czech Academy of Sciences, Institute of Inorganic Chemistry, Husinec-Rez 250 68, Czech Republic*

Aliaksei Vetushka − *The Czech Academy of Sciences, Institute of Physics, 182 21 Prague 8, Czech Republic*

Michal Dušek − *The Czech Academy of Sciences, Institute of Physics, 182 21 Prague 8, Czech Republic;* orcid.org/0000-0001-9797-2559

Jan Macháček − *The Czech Academy of Sciences, Institute of Inorganic Chemistry, Husinec-Rez 250 68, Czech Republic;* orcid.org/0000-0003-4723-0789

Jakub Višnák − *The Czech Academy of Sciences, Institute of Inorganic Chemistry, Husinec-Rez 250 68, Czech Republic; Department of Chemistry, Middle East Technical University, Ankara 06800, Turkey*

Jan Endres − *Department of Condensed Matter Physics, Faculty of Mathematics and Physics, Charles University, 121 16 Praha 2, Czech Republic*

Zdeněk Bastl − *The Czech Academy of Sciences, J. Heyrovsky Institute of Physical Chemistry, 182 23 Prague 8, Czech Republic*

Complete contact information is available at: https://pubs.acs.org/10.1021/acs.chemmater.3c03210

Notes

The authors declare no competing financial interest.

■ ACKNOWLEDGMENTS

E.M.A., K.E.W., and P.S.W. thank the National Science Foundation (grant #CHE-2004238) for support of the self-assembly and surface characterization experiments performed. J.L., J.M., A.V., J.V., J.E., and T.B. thank the Ministry of Education, Youth and Sports of the Czech Republic (MSMT) for the support of the following projects: (1) program Inter-Excellence, subprogram Inter-Action, grant #LTAIN19152; (2) "e-Infrastruktura CZ", grant #e-INFRA CZ LM2018140. Z.B. thanks the Ministry of Education, Youth and Sports of the Czech Republic and the European Regional Development Fund (OP RDE Project: "Carbon Allotropes with Rationalized Nanointerfaces and Nanolinks for Environmental and Biomedical Applications," #CZ.02.1.01/0.0/0.0/16 026/0008382). T.B. and P.S.W. thank the Fulbright Commission for their support of the project "Dipole−Dipole Interactions in Self-Assembled Materials". M.D. thanks the MGML (mgml.eu) infrastructure within the program of Czech Research Infrastructures (grant #LM2018096) for the support of the crystallographic measurements and analyses. E.M. gratefully acknowledges financial support from TUBITAK (The Scientific and Technological Research Council of Turkey, grant #116F174). Calculations reported in this paper were partly performed at TUBITAK ULAKBIM, High Performance and Grid Computing Center (TRUBA resources). A.N.A. acknowledges support from the Department of Energy (BES grant #DE-SC0019152) and the computational resources from the NSF Advanced Cyberinfrastructure Coordination Ecosystem (ACCESS).

■ REFERENCES

(1) Love, J. C.; Estroff, L. A.; Kriebel, J. K.; Nuzzo, R. G.; Whitesides, G. M. Self-Assembled Monolayers of Thiolates on Metals as a Form of Nanotechnology. *Chem. Rev.* **2005**, *105*, 1103−1170.

(2) Ulman, A. Formation and Structure of Self-Assembled Monolayers. *Chem. Rev.* **1996**, *96*, 1533−1554.

(3) Jiang, P.; Deng, K.; Fichou, D.; Xie, S.-S.; Nion, A.; Wang, C. STM Imaging *ortho*- and *para*-Fluorothiophenol Self-Assembled Monolayers on Au(111). *Langmuir* **2009**, *25*, 5012−5017.

(4) Qi, Y.; Liu, X.; Hendriksen, B. L. M.; Navarro, V.; Park, J. Y.; Ratera, I.; Klopp, J. M.; Edder, C.; Himpsel, F. J.; Fréchet, J. M. J.; Haller, E. E.; Salmeron, M. Influence of Molecular Ordering on Electrical and Friction Properties of ω-(*trans*-4-Stilbene)Alkylthiol Self-Assembled Monolayers on Au (111). *Langmuir* **2010**, *26*, 16522−16528.
(5) Liao, L.; Li, Y.; Xu, J.; Geng, Y.; Zhang, J.; Xie, J.; Zeng, Q.; Wang, C. Competitive Influence of Hydrogen Bonding and van Der Waals Interactions on Self-Assembled Monolayers of Stilbene-Based Carboxylic Acid Derivatives. *J. Phys. Chem. C* **2014**, *118*, 28625−28630.
(6) Frey, S.; Stadler, V.; Heister, K.; Eck, W.; Zharnikov, M.; Grunze, M.; Zeysing, B.; Terfort, A. Structure of Thioaromatic Self-Assembled Monolayers on Gold and Silver. *Langmuir* **2001**, *17*, 2408−2415.
(7) Hohman, J. N.; Zhang, P.; Morin, E. I.; Han, P.; Kim, M.; Kurland, A. R.; McClanahan, P. D.; Balema, V. P.; Weiss, P. S. Self-Assembly of Carboranethiol Isomers on Au{111}: Intermolecular Interactions Determined by Molecular Dipole Orientations. *ACS Nano* **2009**, *3*, 527−536.
(8) Yan, J.; Ouyang, R.; Jensen, P. S.; Ascic, E.; Tanner, D.; Mao, B.; Zhang, J.; Tang, C.; Hush, N. S.; Ulstrup, J.; Reimers, J. R. Controlling the Stereochemistry and Regularity of Butanethiol Self-Assembled Monolayers on Au{111}. *J. Am. Chem. Soc.* **2014**, *136*, 17087−17094.
(9) Dameron, A. A.; Ciszek, J. W.; Tour, J. M.; Weiss, P. S. Effects of Hindered Internal Rotation on Packing and Conductance of Self-Assembled Monolayers. *J. Phys. Chem. B* **2004**, *108*, 16761−16767.
(10) Lewis, P. A.; Inman, C. E.; Yao, Y.; Tour, J. M.; Hutchison, J. E.; Weiss, P. S. Mediating Stochastic Switching of Single Molecules Using Chemical Functionality. *J. Am. Chem. Soc.* **2004**, *126*, 12214−12215.
(11) Lewis, P. A.; Inman, C. E.; Maya, F.; Tour, J. M.; Hutchison, J. E.; Weiss, P. S. Molecular Engineering of the Polarity and Interactions of Molecular Electronic Switches. *J. Am. Chem. Soc.* **2005**, *127*, 17421−17426.
(12) Claridge, S. A.; Liao, W.-S.; Thomas, J. C.; Zhao, Y.; Cao, H. H.; Cheunkar, S.; Serino, A. C.; Andrews, A. M.; Weiss, P. S. From the Bottom Up: Dimensional Control and Characterization in Molecular Monolayers. *Chem. Soc. Rev.* **2013**, *42*, 2725−2745.
(13) Goronzy, D. P.; Staněk, J.; Avery, E.; Guo, H.; Bastl, Z.; Dušek, M.; Gallup, N. M.; Gün, S.; Kučeráková, M.; Levandowski, B. J.; Macháček, J.; Šícha, V.; Thomas, J. C.; Yavuz, A.; Houk, K. N.; Danışman, M. F.; Mete, E.; Alexandrova, A. N.; Baše, T.; Weiss, P. S. Influence of Terminal Carboxyl Groups on the Structure and Reactivity of Functionalized *m*-Carboranethiolate Self-Assembled Monolayers. *Chem. Mater.* **2020**, *32*, 6800−6809.
(14) Thomas, J. C.; Goronzy, D. P.; Serino, A. C.; Auluck, H. S.; Irving, O. R.; Jimenez-Izal, E.; Deirmenjian, J. M.; Macháček, J.; Sautet, P.; Alexandrova, A. N.; Baše, T.; Weiss, P. S. Acid−Base Control of Valency within Carboranedithiol Self-Assembled Monolayers: Molecules Do the Can-Can. *ACS Nano* **2018**, *12*, 2211−2221.
(15) Kim, J.; Rim, Y. S.; Liu, Y.; Serino, A. C.; Thomas, J. C.; Chen, H.; Yang, Y.; Weiss, P. S. Interface Control in Organic Electronics Using Mixed Monolayers of Carboranethiol Isomers. *Nano Lett.* **2014**, *14*, 2946−2951.
(16) Schwartz, J. J.; Mendoza, A. M.; Wattanatorn, N.; Zhao, Y.; Nguyen, V. T.; Spokoyny, A. M.; Mirkin, C. A.; Baše, T.; Weiss, P. S. Surface Dipole Control of Liquid Crystal Alignment. *J. Am. Chem. Soc.* **2016**, *138*, 5957−5967.
(17) Thomas, J. C.; Schwartz, J. J.; Hohman, J. N.; Claridge, S. A.; Auluck, H. S.; Serino, A. C.; Spokoyny, A. M.; Tran, G.; Kelly, K. F.; Mirkin, C. A.; Gilles, J.; Osher, S. J.; Weiss, P. S. Defect-Tolerant Aligned Dipoles within Two-Dimensional Plastic Lattices. *ACS Nano* **2015**, *9*, 4734−4742.
(18) Hohman, J. N.; Claridge, S. A.; Kim, M.; Weiss, P. S. Cage Molecules for Self-Assembly. *Mater. Sci. Eng. R Rep.* **2010**, *70*, 188−208.
(19) Li, M.; Wu, H.; Avery, E. M.; Qin, Z.; Goronzy, D. P.; Nguyen, H. D.; Liu, T.; Weiss, P. S.; Hu, Y. Electrically Gated Molecular Thermal Switch. *Science* **2023**, *382*, 585−589.
(20) Cabarcos, O. M.; Shaporenko, A.; Weidner, T.; Uppili, S.; Dake, L. S.; Zharnikov, M.; Allara, D. L. Physical and Electronic Structure Effects of Embedded Dipoles in Self-Assembled Monolayers: Characterization of Mid-Chain Ester Functionalized Alkanethiols on Au{111}. *J. Phys. Chem. C* **2008**, *112*, 10842−10854.
(21) Abu-Husein, T.; Schuster, S.; Egger, D. A.; Kind, M.; Santowski, T.; Wiesner, A.; Chiechi, R.; Zojer, E.; Terfort, A.; Zharnikov, M. The Effects of Embedded Dipoles in Aromatic Self-Assembled Monolayers. *Adv. Funct. Mater.* **2015**, *25*, 3943−3957.
(22) Kang, J. F.; Liao, S.; Jordan, R.; Ulman, A. Mixed Self-Assembled Monolayers of Rigid Biphenyl Thiols: Impact of Solvent and Dipole Moment. *J. Am. Chem. Soc.* **1998**, *120*, 9662−9667.
(23) Kristiansen, K.; Stock, P.; Baimpos, T.; Raman, S.; Harada, J. K.; Israelachvili, J. N.; Valtiner, M. Influence of Molecular Dipole Orientations on Long-Range Exponential Interaction Forces at Hydrophobic Contacts in Aqueous Solutions. *ACS Nano* **2014**, *8*, 10870−10877.
(24) Donhauser, Z. J.; Mantooth, B. A.; Kelly, K. F.; Bumm, L. A.; Monnell, J. D.; Stapleton, J. J.; Price, D. W.; Rawlett, A. M.; Allara, D. L.; Tour, J. M.; Weiss, P. S. Conductance Switching in Single Molecules Through Conformational Changes. *Science* **2001**, *292*, 2303−2307.
(25) Vericat, C.; Vela, M. E.; Benitez, G.; Carro, P.; Salvarezza, R. C. Self-Assembled Monolayers of Thiols and Dithiols on Gold: New Challenges for a Well-Known System. *Chem. Soc. Rev.* **2010**, *39*, 1805.
(26) Mete, E.; Yılmaz, A.; Danışman, M. F. A van der Waals Density Functional Investigation of Carboranethiol Self-Assembled Monolayers on Au{111}. *Phys. Chem. Chem. Phys.* **2016**, *18*, 12920−12927.
(27) Dickerson, P. N.; Hibberd, A. M.; Oncel, N.; Bernasek, S. L. Hydrogen-Bonding versus van der Waals Interactions in Self-Assembled Monolayers of Substituted Isophthalic Acids. *Langmuir* **2010**, *26*, 18155−18161.
(28) Kim, J. Y.; Jang, W. J.; Kim, H.; Yoon, J. K.; Park, J.; Kahng, S.-J.; Lee, J.; Han, S. Supramolecular Interactions of Anthraquinone Networks on Au{111}: Hydrogen Bonds and van Der Waals Interactions. *Appl. Surf. Sci.* **2013**, *268*, 432−435.
(29) Baše, T.; Bastl, Z.; Plzák, Z.; Grygar, T.; Plešek, J.; Carr, M. J.; Malina, V.; Šubrt, J.; Boháček, J.; Večerníková, E.; Kříž, O. Carboranethiol-Modified Gold Surfaces. A Study and Comparison of Modified Cluster and Flat Surfaces. *Langmuir* **2005**, *21*, 7776−7785.
(30) Yeager, L. J.; Saeki, F.; Shelly, K.; Hawthorne, M. F.; Garrell, R. L. A New Class of Self-Assembled Monolayers: *Closo*-$B_{12}H_{11}S^{3-}$ on Gold. *J. Am. Chem. Soc.* **1998**, *120*, 9961−9962.
(31) Alloway, D. M.; Hofmann, M.; Smith, D. L.; Gruhn, N. E.; Graham, A. L.; Colorado, R.; Wysocki, V. H.; Lee, T. R.; Lee, P. A.; Armstrong, N. R. Interface Dipoles Arising from Self-Assembled Monolayers on Gold: UV−Photoemission Studies of Alkanethiols and Partially Fluorinated Alkanethiols. *J. Phys. Chem. B* **2003**, *107*, 11690−11699.
(32) Evans, S. D.; Goppert-Berarducci, K. E.; Urankar, E.; Gerenser, L. J.; Ulman, A.; Snyder, R. G. Monolayers Having Large In-Plane Dipole Moments: Characterization of Sulfone-Containing Self-Assembled Monolayers of Alkanethiols on Gold by Fourier Transform Infrared Spectroscopy, X-Ray Photoelectron Spectroscopy and Wetting. *Langmuir* **1991**, *7*, 2700−2709.
(33) Thomas, J. C.; Goronzy, D. P.; Dragomiretskiy, K.; Zosso, D.; Gilles, J.; Osher, S. J.; Bertozzi, A. L.; Weiss, P. S. Mapping Buried Hydrogen-Bonding Networks. *ACS Nano* **2016**, *10*, 5446−5451.
(34) Baše, T.; Macháček, J.; Hájková, Z.; Langecker, J.; Kennedy, J. D.; Carr, M. J. Thermal Isomerizations of Monothiolated Carboranes $(HS)C_2B_{10}H_{11}$ and the Solid-State Investigation of 9-(HS)-1,2-$C_2B_{10}H_{11}$ and 9-(HS)-1,7-$C_2B_{10}H_{11}$. *J. Organomet. Chem.* **2015**, *798*, 132−140.

https://doi.org/10.1021/acs.chemmater.3c03210
Chem. Mater. 2024, 36, 2085−2095

(35) Kwart, H.; Alekman, S. A Cogwheel Effect in the Internal Rotations of Highly Hindered Systems. *J. Am. Chem. Soc.* **1968**, *90*, 4482−4483.
(36) Lübben, J. F.; Baše, T.; Rupper, P.; Künniger, T.; Macháček, J.; Guimond, S. Tuning the Surface Potential of Ag Surfaces by Chemisorption of Oppositely-Oriented Thiolated Carborane Dipoles. *J. Colloid Interface Sci.* **2011**, *354*, 168−174.
(37) Baše, T.; Bastl, Z.; Šlouf, M.; Klementová, M.; Šubrt, J.; Vetushka, A.; Ledinský, M.; Fejfar, A.; Macháček, J.; Carr, M. J.; Londesborough, M. G. S. Gold Micrometer Crystals Modified with Carboranethiol Derivatives. *J. Phys. Chem. C* **2008**, *112*, 14446−14455.
(38) Thomas, J. C.; Boldog, I.; Auluck, H. S.; Bereciartua, P. J.; Dušek, M.; Macháček, J.; Bastl, Z.; Weiss, P. S.; Baše, T. Self-Assembled *p*-Carborane Analogue of *p*-Mercaptobenzoic Acid on Au{111}. *Chem. Mater.* **2015**, *27*, 5425−5435.
(39) Langecker, J.; Fejfarová, K.; Dušek, M.; Rentsch, D.; Baše, T. Carbon-Substituted 9,12-Dimercapto-1,2-Dicarba-Closo-Dodecaboranes via a 9,12-bis(Methoxy-Methylthio)-1,2-Dicarba-Closo-Dodecaborane Precursor. *Polyhedron* **2012**, *45*, 144−151.
(40) Ferris, J. H.; Kushmerick, J. G.; Johnson, J. A.; Yoshikawa Youngquist, M. G.; Kessinger, R. B.; Kingsbury, H. F.; Weiss, P. S. Design, Operation, and Housing of an Ultrastable, Low Temperature, Ultrahigh Vacuum Scanning Tunneling Microscope. *Rev. Sci. Instrum.* **1998**, *69*, 2691−2695.
(41) Aprà, E.; Bylaska, E. J.; de Jong, W. A.; Govind, N.; Kowalski, K.; Straatsma, T. P.; Valiev, M.; van Dam, H. J. J.; Alexeev, Y.; Anchell, J.; Anisimov, V.; Aquino, F. W.; Atta-Fynn, R.; Autschbach, J.; Bauman, N. P.; Becca, J. C.; Bernholdt, D. E.; Bhaskaran-Nair, K.; Bogatko, S.; Borowski, P.; Boschen, J.; Brabec, J.; Bruner, A.; Cauët, E.; Chen, Y.; Chuev, G. N.; Cramer, C. J.; Daily, J.; Deegan, M. J. O.; Dunning, T. H.; Dupuis, M.; Dyall, K. G.; Fann, G. I.; Fischer, S. A.; Fonari, A.; Früchtl, H.; Gagliardi, L.; Garza, J.; Gawande, N.; Ghosh, S.; Glaesemann, K.; Götz, A. W.; Hammond, J.; Helms, V.; Hermes, E. D.; Hirao, K.; Hirata, S.; Jacquelin, M.; Jensen, L.; Johnson, B. G.; Jónsson, H.; Kendall, R. A.; Klemm, M.; Kobayashi, R.; Konkov, V.; Krishnamoorthy, S.; Krishnan, M.; Lin, Z.; Lins, R. D.; Littlefield, R. J.; Logsdail, A. J.; Lopata, K.; Ma, W.; Marenich, A. V.; Martin del Campo, J.; Mejia-Rodriguez, D.; Moore, J. E.; Mullin, J. M.; Nakajima, T.; Nascimento, D. R.; Nichols, J. A.; Nichols, P. J.; Nieplocha, J.; Otero-de-la-Roza, A.; Palmer, B.; Panyala, A.; Pirojsirikul, T.; Peng, B.; Peverati, R.; Pittner, J.; Pollack, L.; Richard, R. M.; Sadayappan, P.; Schatz, G. C.; Shelton, W. A.; Silverstein, D. W.; Smith, D. M. A.; Soares, T. A.; Song, D.; Swart, M.; Taylor, H. L.; Thomas, G. S.; Tipparaju, V.; Truhlar, D. G.; Tsemekhman, K.; Van Voorhis, T.; Vázquez-Mayagoitia, Á.; Verma, P.; Villa, O.; Vishnu, A.; Vogiatzis, K. D.; Wang, D.; Weare, J. H.; Williamson, M. J.; Windus, T. L.; Woliński, K.; Wong, A. T.; Wu, Q.; Yang, C.; Yu, Q.; Zacharias, M.; Zhang, Z.; Zhao, Y.; Harrison, R. J. NWChem: Past, Present, and Future. *J. Chem. Phys.* **2020**, *152*, 184102.
(42) Johnson, B. G.; Fisch, M. J. An Implementation of Analytic Second Derivatives of the Gradient-corrected Density Functional Energy. *J. Chem. Phys.* **1994**, *100*, 7429−7442.
(43) Adamo, C.; Barone, V. Toward Reliable Density Functional Methods without Adjustable Parameters: The PBE0Model. *J. Chem. Phys.* **1999**, *110*, 6158−6170.
(44) Adamo, C.; Barone, V. Physically Motivated Density Functionals with Improved Performances: The Modified Perdew−Burke−Ernzerhof Model. *J. Chem. Phys.* **2002**, *116*, 5933−5940.
(45) Jensen, F. Unifying General and Segmented Contracted Basis Sets. Segmented Polarization Consistent Basis Sets. *J. Chem. Theory Comput.* **2014**, *10*, 1074−1085.
(46) Yortanlı, M.; Mete, E. Carboxyl- and Amine-Functionalized Carboranethiol SAMs on Au{111}: A Dispersion-Corrected Density Functional Theory Study. *Phys. Rev. Mater.* **2020**, *4*, No. 095002.
(47) Kresse, G.; Furthmüller, J. Efficient Iterative Schemes for *Ab Initio* Total-Energy Calculations Using a Plane-Wave Basis Set. *Phys. Rev. B* **1996**, *54*, 11169−11186.
(48) Kresse, G.; Joubert, D. From Ultrasoft Pseudopotentials to the Projector Augmented-Wave Method. *Phys. Rev. B* **1999**, *59*, 1758−1775.
(49) Blöchl, P. E. Projector Augmented-Wave Method. *Phys. Rev. B* **1994**, *50*, 17953−17979.
(50) Sun, J.; Ruzsinszky, A.; Perdew, J. P. Strongly Constrained and Appropriately Normed Semilocal Density Functional. *Phys. Rev. Lett.* **2015**, *115*, No. 036402.
(51) Vydrov, O. A.; Van Voorhis, T. Nonlocal van Der Waals Density Functional: The Simpler the Better. *J. Chem. Phys.* **2010**, *133*, 244103.
(52) Peng, H.; Yang, Z.-H.; Perdew, J. P.; Sun, J. Versatile van Der Waals Density Functional Based on a Meta-Generalized Gradient Approximation. *Phys. Rev. X* **2016**, *6*, No. 041005.
(53) Yortanlı, M.; Mete, E. Common Surface Structures of Graphene and Au{111}: The Effect of Rotational Angle on Adsorption and Electronic Properties. *J. Chem. Phys.* **2019**, *151*, 214701.
(54) Ferrighi, L.; Madsen, G. K. H.; Hammer, B. Self-Consistent Meta-Generalized Gradient Approximation Study of Adsorption of Aromatic Molecules on Noble Metal Surfaces. *J. Chem. Phys.* **2011**, *135*, No. 084704.
(55) Shepard, S.; Smeu, M. First Principles Study of Graphene on Metals with the SCAN and SCAN+rVV10 Functionals. *J. Chem. Phys.* **2019**, *150*, 154702.
(56) Yeh, I.-C.; Berkowitz, M. L. Ewald Summation for Systems with Slab Geometry. *J. Chem. Phys.* **1999**, *111*, 3155−3162.

https://doi.org/10.1021/acs.chemmater.3c03210
Chem. Mater. 2024, 36, 2085−2095